

Analysis of vibration characteristics of opening device for deepwater robot cabin door and study of its structural optimization design

Baoping Zeng¹, Jipeng Liu², Yu Zhang¹, Yajun Gong¹, Sanbao Hu^{2,*}

¹ 201 Research Group, Wuhan 2nd Ship Research & Design Institute, Wuhan, 430064, China;

² School of Vehicle Engineering, Wuhan University of Technology, Wuhan, 430070, China.

*Corresponding Author: 14093070@qq.com.

Abstract. Deepwater robots are important devices for human to explore the sea, which is being under development towards intellectualization, multitasking, long-endurance and large depth along with the development of science and technology. As far as a deep-water robot is concerned, its mechanical systems is an important subsystem because not only it influences the instrument measuring precision and shorten the service life of cabin devices but also its overlarge vibration and noise lead to disadvantageous effects to marine life within the operational area. Therefore, vibration characteristics shall be key factor for the deep-water robot system design. The sample collection and recycling system of some certain deepwater robot in a mechanism for opening the underwater cabin door for external operation and recycling test equipment is focused in this study. For improving vibration characteristics of locations of the cabin door during opening processes, a vibration model was established to the opening system; and the structural optimization design was carried out to its important structures by utilizing the multi-objective shape optimization and topology optimization method based on analysis of the system vibration. Analysis of characteristics of exciting forces causing vibration was first carried out, which include characteristics of dynamic loads within the hinge clearances and due to friction effects and the fluid dynamic exciting forces during processes of opening the cabin door. Moreover, vibration acceleration responses for a few important locations of the devices for opening the cabin cover were deduced by utilizing the modal synthesis method so that its rigidity and modal frequency may be one primary factor influencing the system vibration performances based on analysis of weighted acceleration responses. Thus, optimization design was carried out to the cabin cover by utilizing the multi-objective topology optimization method to perform reduction of weighted accelerations of key structure locations.

1. Introduction

Deepwater robots are a kind of important equipment for human being to go in for ocean exploration, which is being under development towards intellectualization, multitasking, long-endurance and large



depth along with the development of science and technology. As far as a deep-water robot is concerned, its mechanical systems is an important subsystem because not only it influences the instrument measuring precision and shorten the service life of cabin devices but also its overlarge vibration and noise lead to disadvantageous effects to marine life within the operational area. Therefore, vibration characteristics shall be key factor for the deep-water robot system design. Our mechanism is a part of the sample collection and recycling system of some certain deepwater robot in a mechanism for opening the underwater cabin door for external operation and recycling test equipment. For improving its vibration characteristics, the multi-objective bead topology optimization method was utilized in this study to perform optimization design to important structures of the system. We presented a research overview of related fields to let readers better understand our research contents.

1.1. Development of deepwater robots and the corresponding sample recycling system

Deepwater robots existed for the first time since the 1950s and they are constantly updated for more than half a century to achieve the remarkable development. Man-carrying underwater vehicles, cable remote control and wireless control underwater vehicles and compound pattern underwater vehicles appeared successively. Early deepwater robots were primarily utilized in the military field and USA technology was the most advanced. Afterwards, deepwater robots (such as UK Sub-Atlantic COMANCHE small deepwater robots [1], China CR-01A 6000m unmanned wireless remote underwater vehicles (1990s) and current excellent Jiaolong deep-sea vehicles) were utilized for exploration of underwater energy materials in many countries along with reduction of land available resources; and the successful development of these high performance deepwater robots provides a platform for the specific study of seabed materials; moreover, a broader space for the development of deepwater robots will be provided along with the further development of those technologies such as communication technology in future.

Further study and utilization of abundant marine resources shall first need sample recycling of marine sediment. However, the complexity of marine environment prevents our deeper ocean research and analysis. For solving such issue, people have developed a variety of automatic sampling recovery devices, such as Yngve Kristoffersen's seabed samplers based on the sea static pressure principle [2], Temdoug Somsiri's easily operated and highly integrated seabed sediment samplers [3] and RICHARD A. JAHNKE's multifunctional piston samplers with hydraulic pumps based on the gravity driving principle equipped in deepwater robots.

1.2. Topology optimization design method for vibration structures

At present, there are many vibration attenuation measures for structures, and the vibration attenuation design by utilizing the topology and bead optimization methods is a new method and thought. The primary thought of the vibration attenuation design based on the topology optimization method starts changing the topology of a structure for optimization and configuration of its mass and stiffness characteristics in accordance with the optimal topology structure distributed material; thus, the structure inherent frequency may be improved to be far away from its excitation frequency and prevent any resonance. On the other hand, the primary thought of the vibration attenuation design based on the bead optimization method is to obtain the optimal reinforcement distribution of a structure through the bead optimization; thus, the amplitude of its inherent frequency may be further improved, and the original structure stiffness may be strengthened. Its aims are to improve vibration performances of underwater structures, realize the structure application effectiveness and the optimal combination of vibration characteristics.

1.3. Engineering application of the topology optimization method of vibration characteristics

Currently, many scholars at home and abroad have studied the multi-objective topology and bead optimization theory and application issues. Niels Colhoff et al. optimized plate structures by utilizing the structure stiffness and frequency as targets [4]. Seungjae Min et al. studied the multi-objective

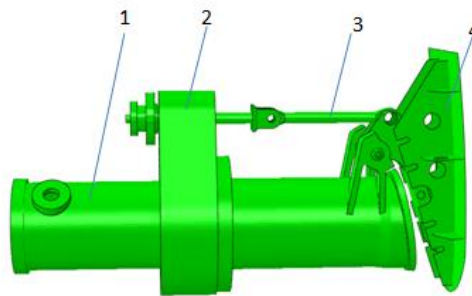
topology optimization issue based on their static stiffness and dynamic vibration frequency [5]. Murali M.R. Krishna studied the bead optimization issues for automobile power transmission shafts by taking the structure inherent frequency as the target [6]. Yang Dai and Das M. Ramanathan al. utilized the bead optimization technology to meet the vibration attenuation and noise reduction requirements of the transmission shafts [7].

The topology optimization was carried out to cover plates of underwater mechanisms to improve vibration characteristics of the whole system based on comprehensive consideration of movement relations between underwater structures and effects of the system vibration and the fluid excitation during the operating processes and by utilizing the multi-objective topology optimization method in this study.

2. Analysis of the system vibration characteristics

2.1. System composition and operating principle

An underwater mechanism as an important sub-system of a deepwater robot is primarily to serve the sampling and recycling system, which is shown in Figure 1; and the system is primarily made up of a cover plate and a barrel. An operating period of the system is as follows: the cover plate is driven by the tie rod to rotate around the shaft; at the same time, the sampling mechanical arm extends from the barrel; then it is taken back after sampling; and the cover plate is closed to complete the sample recycling process.



1: Barrel; 2: Mounting support; 3: Transmission tie rod; 4: Cover plate.

Figure 1. Structure schematic diagram of an underwater mechanism

2.2. Analysis of characteristics of vibration sources

It is known through analysis of the mechanism operating principle that the cover plate as a primary operating part of the system is in direct contact to its surrounding fluid during the actual operating processes, when its whole forward movement occurs along with that of the robot and it is driven by the tie rod to rotate around the connecting pin; thus, the cover plate is acted by not only the mechanical excitation from the mechanism but also the external fluid excitation during its opening or closing process; moreover, the rotation speed of the cover plate, the stiffness of each part of the system, the friction and clearance between joints and fluid velocity and so on may influence the excitation of the cover plate. Due to the highly coupling effect between the cover plate and fluid during the motion processes, the vibration and spoiling effects of the cover plate may change its surrounding flow field so that the intensive turbulence effect of fluid may occur at the tip of the cover plate; on the other hand, the changing fluid may result in the complicated flow-induced effect to the cover plate; moreover, such excitation frequency being within a frequency band is one of important causes for the structure resonance. Thus, the structure optimization was carried out to the part dominating the system vibration performances based on the theoretical analysis in this study to improve vibration performances of the system for opening the cabin door.

2.3. Mathematical model for analysis of the system vibration responses

The dynamic substructure method as a new numerical simulation method has unique advantages for analysis of dynamic characteristics of any complicated structure, which may be used to reduce a calculation model including huge DOFs into the one including only a few DOFs and easy for analysis [8] so that the computational efficiency may be greatly improved. This method is derived from the supposing substructure modal synthesis method put forward by Hurty in 1960s [9]. Subsequently, Glad Well put forward the component modal synthesis method [10] and Hurty constructed based on the point of kinematics and Ritz put forward the thought of the fixed interface component mode synthesis method [11]. Craig and Bampton improved Hurty's method in 1968 to put forward a complete mode set being made up of low order predominant modes retained in the fixed interfaces of substructures and constraint modes of all interface DOFs, and this serves as the supposing mode C-B method of the whole system [12]; thus, the dynamic substructure method became more simplified and practical. The development of the dynamic substructure method has let its theory be further perfected and developed so far along with the rapid development of the computer technology; and the scope of application of this method also extends to the dynamic interaction study between structures and surrounding media from the former dynamic analysis of general structures or systems.

The dynamic substructure method focuses “first modification and then recovery”; namely, the entire system is first divided into sub-systems which are independent and easy for analysis, and the modal parameters of each sub-system are calculated the vibration characteristics of each sub-system are split by utilizing the modal coordinates. Then, the motion equations of the entire system may be established under the modal coordinates in accordance with constraint conditions in each sub-system connection surfaces to obtain the modal parameters of the entire structure system. Because the C-B mode synthesis method is relatively easy to understand, and no suspending substructure may occur in analysis, analysis of dynamic characteristics of the underwater structure was carried out by utilizing our method to find out the maximum influencing factor for the system vibration performances.

(1) First of all, the entire mechanism is divided into the tie rod, the barrel cover plate and 3 substructures (namely Substructures A, B and C) in the cover plate rotating joint; and the cover plate is connected with the tie rod and the barrel. It is shown in Figure 2.

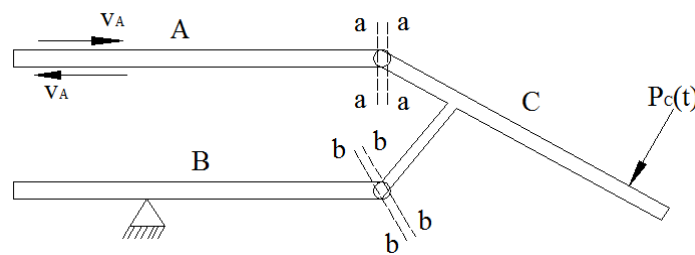


Figure 2. Simplified motion diagram of the system structure ($p_c(t)$ represents the fluid excitation)

(2) The motion equation of the Substructure tie rod is expressed as:

$$\begin{bmatrix} m_A^{ii} & m_A^{ia} \\ m_A^{ai} & m_A^{aa} \end{bmatrix} \begin{Bmatrix} \ddot{u}_A^i \\ \ddot{u}_A^a \end{Bmatrix} + \begin{bmatrix} m_A^{ii} & k_A^{ia} \\ k_A^{ai} & k_A^{aa} \end{bmatrix} \begin{Bmatrix} u_A^i \\ u_A^a \end{Bmatrix} = \begin{Bmatrix} p_A^i(t) \\ p_A^a(t) \end{Bmatrix} \quad (1)$$

Where: i and a represent the DOF set of the non-crosslinked interfaces of the substructure and the DOF set of the crosslinked interfaces of the substructure, respectively; $p_A^a(t)$ and $p_A^i(t)$ represent the force in the linking boundary between Substructures A and C and the external force in the internal DOFs of Substructure A.

The predominant modal matrix $[\Phi_A]$ of Substructure A may be calculated by the following equation:

$$([\mathbf{k}_A^{ii}] - \lambda [\mathbf{m}_A^{ii}]) \{\Phi_A\} = \{0\} \quad (j = 1, 2, \dots, n_A^k) \quad (2)$$

The constrained matrix $[\psi_A]$ of Substructure A may be solved by:

$$[\psi_A] = -[\mathbf{k}_A^{ii}]^{-1} [\mathbf{k}_A^{ia}] \quad (3)$$

The corresponding transfer matrix is:

$$[T_A] = \begin{bmatrix} \Phi_k & \psi_A \\ 0 & I \end{bmatrix} \quad (4)$$

Where: $[\Phi_k]$ represents the reduced predominant modal matrix of Substructure A, where k represents the number of the reserved low order predominant modes of Substructure A. The dynamic displacement of Substructure A is expressed by:

$$\begin{Bmatrix} u_A^k \\ u_A^a \end{Bmatrix} = [T_A] \begin{Bmatrix} q_A^k \\ u_A^a \end{Bmatrix} = \begin{bmatrix} \Phi_k & \psi_A \\ 0 & I \end{bmatrix} \begin{Bmatrix} q_A^k \\ u_A^a \end{Bmatrix} \quad (5)$$

The undamped motion equation of Substructure A under the modal coordinates is:

$$[\tilde{M}_A] \begin{Bmatrix} \ddot{q}_A^k \\ \ddot{u}_A^a \end{Bmatrix} + [\tilde{K}_A] \begin{Bmatrix} q_A^k \\ u_A^a \end{Bmatrix} = \{\tilde{p}_A(t)\} \quad (6)$$

Where: the vector sets of the corresponding mass and stiffness matrixes and the external force are:

$$[\tilde{M}_A] = \begin{bmatrix} I_A^{kk} & \tilde{m}_A^{ka} \\ \tilde{m}_A^{ak} & \tilde{m}_A^{aa} \end{bmatrix} = [T_A]^T [M_A] [T_A] \quad (7)$$

$$[\tilde{K}_A] = \begin{bmatrix} \Lambda_A^{kk} & 0 \\ 0 & \tilde{k}_A^{aa} \end{bmatrix} = [T_A]^T [K_A] [T_A] \quad (8)$$

$$\{\tilde{p}_A(t)\} = [T_A]^T \begin{Bmatrix} p_A^i(t) \\ p_A^a(t) \end{Bmatrix} = \begin{Bmatrix} \{[\Phi_k]^T p_A^i(t)\} \\ \{[\psi_A]^T p_A^i(t) + p_A^a(t)\} \end{Bmatrix} \quad (9)$$

(3) Similarly, the undamped motion equation of Substructure B under the modal coordinates is:

$$[\tilde{M}_B] \begin{Bmatrix} \ddot{q}_B^l \\ \ddot{u}_B^a \end{Bmatrix} + [\tilde{K}_B] \begin{Bmatrix} q_B^l \\ u_B^a \end{Bmatrix} = \{\tilde{p}_B(t)\} \quad (10)$$

Where: the vector sets of the corresponding mass and stiffness matrixes and the external force are:

$$[\tilde{M}_B] = \begin{bmatrix} I_B^{ll} & \tilde{m}_B^{lb} \\ \tilde{m}_B^{bl} & \tilde{m}_B^{bb} \end{bmatrix} = [T_B]^T [M_B] [T_B] \quad (11)$$

$$[\tilde{K}_B] = \begin{bmatrix} \Lambda_B^{ll} & 0 \\ 0 & \tilde{k}_B^{bb} \end{bmatrix} = [T_B]^T [K_B] [T_B] \quad (12)$$

$$\{\tilde{p}_B(t)\} = [T_B]^T \begin{Bmatrix} p_B^i(t) \\ p_B^a(t) \end{Bmatrix} = \begin{Bmatrix} [\Phi_l]^T p_B^i(t) \\ [\psi_B]^T p_B^i(t) + p_B^a(t) \end{Bmatrix} \quad (13)$$

(4) The corresponding transfer matrix is:

$$[T_B] = \begin{bmatrix} \Phi_l & \psi_B \\ 0 & I \end{bmatrix} \quad (14)$$

Where: $[\Phi_l]$ represents the reduced predominant modal matrix of Substructure B, where l represents the number of the reserved low order predominant modes of Substructure B.

(5) As for Substructure cover plate, its mass, stiffness and load matrixes are divided into blocks in accordance with DOFs of crosslinked and non-crosslinked interfaces, and its undamped free vibration equation is expressed by:

$$\begin{bmatrix} m_C^{ii} & m_C^{ia} & m_C^{ib} \\ m_C^{ai} & m_C^{aa} & m_C^{ab} \\ m_C^{ii} & m_C^{ba} & m_C^{bb} \end{bmatrix} \begin{Bmatrix} \ddot{u}_C^i \\ \ddot{u}_C^a \\ \ddot{u}_C^b \end{Bmatrix} + \begin{bmatrix} k_C^{ii} & k_C^{ia} & k_C^{ib} \\ k_C^{ai} & k_C^{aa} & k_C^{ab} \\ k_C^{ii} & k_C^{ba} & k_C^{bb} \end{bmatrix} \begin{Bmatrix} u_C^i \\ u_C^a \\ u_C^b \end{Bmatrix} = \begin{Bmatrix} p_C^i(t) \\ p_C^a(t) \\ p_C^b(t) \end{Bmatrix} \quad (15)$$

Where: $p_C^i(t)$ represents the fluid excitation of the cover plate; $p_C^a(t)$ and $p_C^b(t)$ represent the mechanism excitation effects due to hinging impacts between the cover plate and tie rod, and the cover plate and the barrel joint, respectively.

While assuming Substructures C, A and B are fully fixed in their crosslinked interfaces (namely $u_C^a = 0$ and $u_C^b = 0$), the predominant modal matrix $[\Phi_C]$ of Substructure C may be solved by the following equation:

$$([k_C^{ii}] - \lambda [m_C^{ii}]) \{\Phi_C\} = \{0\} \quad (j = 1, 2, \dots, n_C^m) \quad (16)$$

While the displacement and acceleration of the substructure nodes in Equation (2-16) are 0 and the unit displacement is taken to a some certain DOF of the crosslinked interfaces of Substructures C, A

and B in turn, and other DOFs of the crosslinked interfaces are completely fixed, the constraint modal matrix of Substructure C may be solved by:

$$\begin{bmatrix} \psi_C^{ia} \end{bmatrix} = -\begin{bmatrix} k_C^{ii} \end{bmatrix}^{-1} \begin{bmatrix} k_C^{ia} \end{bmatrix} \quad (17)$$

$$\begin{bmatrix} \psi_C^{ib} \end{bmatrix} = -\begin{bmatrix} k_C^{ii} \end{bmatrix}^{-1} \begin{bmatrix} k_C^{ib} \end{bmatrix} \quad (18)$$

The corresponding transfer matrix of Substructure C is:

$$\begin{bmatrix} T_C \end{bmatrix} = \begin{bmatrix} \Phi_m & \psi_C^{ia} & \psi_C^{ib} \\ 0 & I^{ia} & 0 \\ 0 & 0 & I^{ib} \end{bmatrix} \quad (19)$$

Where: $\begin{bmatrix} \Phi_m \end{bmatrix}$ represents the reduced predominant modal matrix of Substructure C, where m represents the number of the reserved low order predominant modes of Substructure C. The dynamic displacement of Substructure A is:

$$\begin{Bmatrix} u_C^m \\ u_C^a \\ u_C^b \end{Bmatrix} = \begin{bmatrix} T_C \end{bmatrix} \begin{Bmatrix} q_C^m \\ u_C^a \\ u_C^b \end{Bmatrix} \quad (20)$$

The undamped motion equation of Substructure C under the modal coordinates is:

$$\begin{bmatrix} \tilde{M}_C \end{bmatrix} \begin{Bmatrix} \ddot{q}_C^m \\ u_C^a \\ u_C^b \end{Bmatrix} + \begin{bmatrix} \tilde{K}_C \end{bmatrix} \begin{Bmatrix} q_C^m \\ u_C^a \\ u_C^b \end{Bmatrix} = \{ \tilde{p}_C(t) \} \quad (21)$$

Where: the vector sets of the corresponding mass and stiffness matrixes and the external force are:

$$\begin{bmatrix} \tilde{M}_C \end{bmatrix} = \begin{bmatrix} T_C \end{bmatrix}^T \begin{bmatrix} M_C \end{bmatrix} \begin{bmatrix} T_C \end{bmatrix} = \begin{bmatrix} I_C^{mm} & \tilde{m}_C^{ma} & \tilde{m}_C^{mb} \\ \tilde{m}_C^{am} & \tilde{m}_C^{aa} & \tilde{m}_C^{ab} \\ \tilde{m}_C^{bm} & \tilde{m}_C^{ba} & \tilde{m}_C^{bb} \end{bmatrix} \quad (22)$$

$$\begin{bmatrix} \tilde{K}_C \end{bmatrix} = \begin{bmatrix} T_C \end{bmatrix}^T \begin{bmatrix} K_C \end{bmatrix} \begin{bmatrix} T_C \end{bmatrix} = \begin{bmatrix} \Lambda_C^m & 0 & 0 \\ 0 & \tilde{k}_C^{aa} & 0 \\ 0 & 0 & \tilde{k}_C^{bb} \end{bmatrix} \quad (23)$$

$$\{\tilde{p}_c(t)\} = [T_c]^T \begin{Bmatrix} p_c^i(t) \\ p_c^a(t) \\ p_c^b(t) \end{Bmatrix} = \begin{Bmatrix} \{[\Phi_i]^T p_c^i(t)\} \\ \{[\psi_c^{ia}]^T p_c^i(t) + p_c^a(t)\} \\ \{[\psi_c^{ib}]^T p_c^i(t) + p_c^b(t)\} \end{Bmatrix} \quad (24)$$

(6) In accordance with compatibility conditions of forces and displacements of crosslinked interfaces of various substructures, namely:

$$u_A^a = u_C^a = q^a, \quad u_B^b = u_C^b = q^b, \quad p_A^a(t) + p_C^a(t) = 0 \quad \text{and} \quad p_B^b(t) + p_C^b(t) = 0 \quad (25)$$

Where: q^a and q^b represent the modal coordinates of nodes in crosslinked interfaces between Substructures A and C and Substructures B and C. The undamped motion equations of the system including 3 substructures under the modal coordinates may be derived by simultaneous solution of the above equations.

$$[M] \begin{Bmatrix} \ddot{q}_A^k \\ \ddot{q}_C^m \\ \ddot{q}_B^l \\ \ddot{q}^a \\ \ddot{q}^b \end{Bmatrix} + [K] \begin{Bmatrix} q_A^k \\ q_C^m \\ q_B^l \\ q^a \\ q^b \end{Bmatrix} = \{\bar{p}(t)\} \quad (26)$$

Where:

$$[M] = \begin{bmatrix} I_A^{kk} & 0 & 0 & \tilde{m}_A^{ka} & 0 \\ 0 & I_C^{mm} & 0 & \tilde{m}_C^{ma} & \tilde{m}_C^{mb} \\ 0 & 0 & I_B^{ll} & 0 & \tilde{m}_B^{lb} \\ \tilde{m}_A^{ak} & \tilde{m}_C^{am} & 0 & \tilde{m}_A^{aa} + \tilde{m}_C^{aa} & \tilde{m}_C^{ab} \\ 0 & \tilde{m}_C^{bm} & \tilde{m}_B^{bl} & \tilde{m}_C^{ba} & \tilde{m}_C^{bb} + \tilde{m}_B^{bb} \end{bmatrix}$$

$$[K] = \begin{bmatrix} \Lambda_A^{kk} & 0 & 0 & 0 & 0 \\ 0 & \Lambda_C^{mm} & 0 & 0 & 0 \\ 0 & 0 & \Lambda_B^{ll} & 0 & 0 \\ 0 & 0 & 0 & \tilde{k}_A^{aa} + \tilde{k}_C^{aa} & 0 \\ 0 & 0 & 0 & 0 & \tilde{k}_C^{bb} + \tilde{k}_B^{bb} \end{bmatrix}$$

$$\{\bar{p}(t)\} = \left\{ \begin{array}{l} \{\Phi_k\}^T p_A^i(t) \\ \{\Phi_m\}^T p_C^i(t) \\ \{\Phi_l\}^T p_B^i(t) \\ \{\psi_A\}^T p_A^i(t) + \{\psi_C^{ia}\}^T p_C^i(t) \\ \{\psi_B\}^T p_B^i(t) + \{\psi_C^{ib}\}^T p_C^i(t) \end{array} \right\}$$

Equation (2-28) may be decoupled and solved to obtain the vibration response of the system under the modal coordinates which may be converted into generalized coordinates initially selected for the system by the transfer matrixes $[T_A]$, $[T_B]$ and $[T_C]$. The system damping effects are not taken into account during the above derivation processes. As for a small damping engineering system, the system damping may be assumed to meet the proportional damping relationship (namely: $[C] = \alpha[M] + \beta[K]$, α and β are constant scalars), Equation (2-28) may be converted into:

$$[M] \left\{ \begin{array}{l} \ddot{q}_A^k \\ \ddot{q}_C^m \\ \ddot{q}_B^l \\ \ddot{q}^a \\ \ddot{q}^b \end{array} \right\} + [K] \left\{ \begin{array}{l} q_A^k \\ q_C^m \\ q_B^l \\ q^a \\ q^b \end{array} \right\} + [C] \left\{ \begin{array}{l} \dot{q}_A^k \\ \dot{q}_C^m \\ \dot{q}_B^l \\ \dot{q}^a \\ \dot{q}^b \end{array} \right\} = \{\bar{p}(t)\} \quad (27)$$

3. Establishment of the optimization model for any mechanism facing vibration control

It is known from Equation (2-29) that the system structure modes are an important factor for determining the size of the vibration response. Due to the cover plate belonging to sheet structures and its modal frequency being relatively small and the mode density being large, it provides more contributions to vibration of the entire system. Thus, the vibration acceleration of the hinging end far away from the cover plate is selected in the engineering practice to evaluate the system vibration. Structure optimization was carried out to the cover plate here to improve its structure stiffness and various-order modal frequencies below 2000Hz.

3.1. Establishment of the optimization model for optimization of the cover plate structure

The topology optimization technology as the most promising and innovative one in the structure optimization technologies is to seek the optimal material distribution or force transmission path in the given design region in accordance with the given load and constraint conditions and performance indexes; moreover, the topology optimization focuses the material interpolation model whose common forms are the homogenization method and the variable density method (SIMP). The variable density interpolation model was used here; namely, an assumed unit relative density was introduced and the relationship between the elasticity modulus and the relative density of each unit in the design space was characterized by an empirical formula [13]; and the assumed relative density of each unit acts as a design variable; thus, the topology optimization issue of a structure may be converted into a material distribution issue. For getting clearer an optimization results, a penalty factor is introduced into the empirical formula on the design variables and the unit elasticity modulus to punish the unit intermediate density and let the unit density tend to 0 or 1. The SIMP material interpolation model [14] is as follows:

$$E_i(\rho) = \rho_i^p E_0$$

Where: ρ_i represents the unit relative density; p represents the penalty factor, which is generally taken as 3; E_0 represents the material elasticity modulus; and $E_i(\rho)$ represent the elasticity modulus of the i^{th} unit.

Because our optimization targets are to seek maximizing the cover plate stiffness and each-order inherent frequency (≤ 45 orders) is no less than that of the original structure, it is a multi-objective optimization issue; whereas, the general topology optimization software can only utilized to deal with the single-objective issues; thus, the multi-objective optimization issue shall be converted into a single-objective issue. The common method for performing such conversion process is to set one target as a constraint condition and the other target as a target function. Each-order modal frequency (≤ 45 orders) which is no less than that of the original structure here is set as a constraint condition; thus, modal analysis shall be carried out to the structure prior to optimization to calculate each-order inherent frequency of the cover plate (≤ 45 orders). Because maximizing the structure stiffness may be equivalent to minimizing its flexibility which may be defined by the strain energy; thus, our target function is to minimize the strain energy of the cover plate.

Based on the SIMP method, the mathematical model for the topology optimization issue (maximizing the cover plate stiffness) may be expressed by [15]:

$$\begin{aligned} \min : c(\rho) &= \sum_{i=1}^n E_0 \rho_i^p u_e^T k_0 u_e \\ \text{subject to: } &\frac{V(\rho)}{V_0} = V_{ol}, \\ &f_n \geq \bar{f}_n (n=1, 2, 3, \dots, 45) \\ &KU=F; 0 \leq \rho_{\min} \leq \rho \leq 1 \end{aligned}$$

Where: $c(\rho)$ represent the strain energy; u_e and k_0 represent the unit displacement vector and stiffness matrix, respectively; $V(\rho)$ and V_0 represent the design space optimization volume and design control initial volume, respectively; V_{ol} represents the design region volume fractions before or after optimization; \bar{f}_n represents each-order inherent frequency of the structure prior to optimization; U and F represent the overall displacement and force vectors, respectively; K represents the overall stiffness matrix; and ρ_{\min} represents the minimum unit relative density which shall necessarily be satisfied to avoid any stiffness singularity.

The above topology optimization issue may be solved by a few methods such as the optimum criterion method (OC), the sequential linear programming algorithm (SLP) and the method of moving asymptotes (MMA). The optimum criterion method (OC) was utilized here to solve the topology optimization issue (maximizing the cover plate stiffness). While applying the optimum criterion method (OC), the sensitivity of the target function is necessarily solved, which is expressed as:

$$\frac{\partial c}{\partial \rho_i} = -p \rho_i^{p-1} u_e^T k_0 u_e E_0$$

3.2. Optimization method and numerical instability treatment

The numerical instability issues (primarily including the checkerboard phenomenon and the mesh-dependence) may easily occur while performing the topology optimization. The checkerboard phenomenon may lead to unclear optimization results and production of processing mode shape

residual; on the other hand, the mesh-dependence may result in lowering the reliability of calculation results. It is very important to eliminate the numerical instability issues such as the checkerboard phenomenon and the mesh-dependence in the topology optimization processes and it is directly related to the reliability of the optimization results and workability. Such two instability phenomena generally coexist in optimization results; and those methods for effectively eliminating the checkerboard phenomenon may also be utilized to effectively eliminate the mesh-dependence issues. In view of these instability phenomena, O. Sigmund [16] carried out a thorough research and put forward a few solutions such as the grid filtration method, the perimeter constraint method and the local gradient constraint method.

The grid filtration method was utilized here in the topology optimization processes to effectively eliminate the checkerboard phenomenon and the mesh-dependence, which is based on correction of the sensitivity information of the target function [17]:

$$\frac{\partial \bar{c}}{\partial \rho_i} = \frac{1}{\max(\gamma, \rho_i) \sum_{i \in N_e} H_{ei}} \sum_{i \in N_e} H_{ei} \rho_i \frac{\partial c}{\partial \rho_i}$$

$$H_{ei} = \max(0, r_{\min} - \Delta(e, i))$$

Where: N_e represents the unit set within $\Delta(e, i)$ from the center of Unit e ; r_{\min} represents the filtration radius; H_{ei} represents the weight coefficient; and $\gamma (= 10^{-3})$ is a very small positive number which is to prevent any design variable being equal to 0.

3.3. Establishment of the topology optimization model for cover plates

The bead and topology optimization methods belong to the structure concept design method, whose theoretical base and solving methods are also similar. The bead optimization method is primarily utilized to seek the optimal stiffeners distribution in sheet structures to reduce the structure deformation and vibration, and improve the modal frequency. The bead optimization was first carried out to cover plate here to obtain the specific distribution locations of stiffeners prior to starting the topology optimization; and then topology optimization was carried out to the cover plate to obtain the optimal material distribution.

The optimization model was established here based on Hypermesh to the cover plate, which is shown in Figure 3. Because various parts of the cover plate belong to thin-wall structures, shell units were utilized to simulate the entire cover plate model during the modeling processes; and the FE model includes 9184 units in total. The static load and mode sub-operating conditions are necessarily established in the bead and topology optimization models, where the load is set as 0.01MPa and the action region is located in the semicircular region at the top of the cover plate; and the mode operating condition is set as the early 30-order modes. The constraint condition is set as the mean value of the early 30-order inherent frequencies of the cover plate is no less than that of the structure prior to optimization; and the target function is set as minimizing the strain energy of the cover plate. The bead optimization region is the base of the cover plate and the topology optimization region is the base and 2 longitudinal members of the cover plate. The maximum draft angle, the maximum reinforcement height and the minimum reinforcement width are set as 60°, 20mm and 20mm in the bead optimization model, respectively. The design region volume fraction is set as $f = 0.5$ in the topology optimization model; moreover, the minimum member size is set as 20mm to eliminate any tiny force transmission path in the topology optimization results.

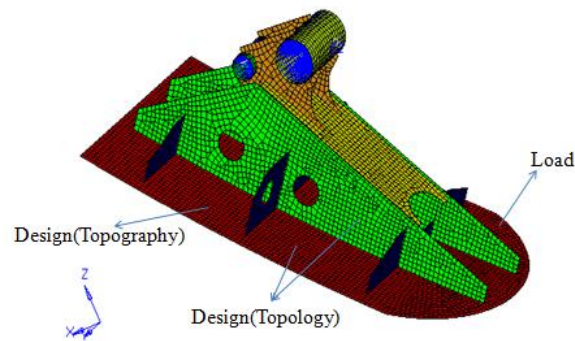


Figure 3. Cover plate bead and topology optimization model

4. Optimization results and verification

4.1. Bead optimization results and analysis

The results are convergent after optimization iteration for 75 times. The bead optimization results for the base of the cover plate are shown in Figure 4, where the red part is the location for designing a boss in the subsequent optimization design to enhance the cover plate stiffness and the blue part is region which may not be deformed (namely this location may not be reinforced). It is known from Figure 4 that the optimizing region of the cover plate is primarily centralized in the front edge of the base because this region is at the forced boundary and the top end of the base is far away from the rotating point of the cover plate so that relatively large vibration might occur even if the cover plate was under a relatively small vibration speed; and such Figure also indicates that the maximum height for processing a boss is 20mm. Figure 5. is an iteration curve of the cover plate flexibility during the bead optimization processes, from which it is known that the cover plate flexibility is reduced to 23.5N·mm from 55N·mm after iteration for 75times; and such case indicates by combining the bead optimization results that stiffeners may be processed in the corresponding locations of the base of the cover plate and the cover plate stiffness may be greatly improved; thus, the cover plate vibration may be reduced and the system vibration performances may be improved in the actual operating processes.

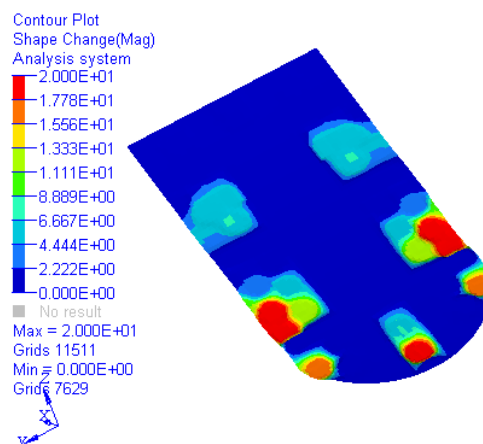


Figure 4. Bead optimization results for the base

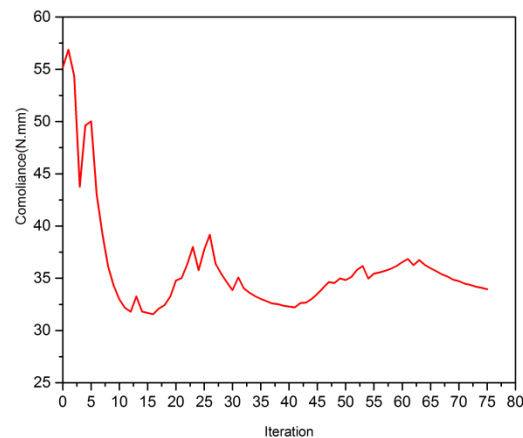


Figure 5. Bead optimization iteration process curve

4.2. Topology optimization results and analysis

The results are convergent after 80 iteration steps and the topology optimization results are shown in Figures 6 and 7, where the red part and its neighbouring parts are force transmission paths which must be reserved in the subsequent optimization design and the blue part and its neighbouring parts are unimportant regions which may be removed in the subsequent optimization design processes to achieve the lightweight of structures. Figure 6 indicates that the force transmission path is just through the round hole at the top of the longitudinal member while the part with low density is removed by changing the unit density threshold; and such case indicates that such round hole is under the irrational design so that the cover plate stiffness may be greatly weakened, and it points out an important direction for the subsequent optimization design. Figure 7 indicates that the optimizing region of the base is primarily centralized in the edge of the rear semi-half part of the base primarily due to the excitation force (fluid turbulence effect) of the front semi-half part of the base while the red part and its neighbouring parts are only be reserved by changing the unit density threshold.

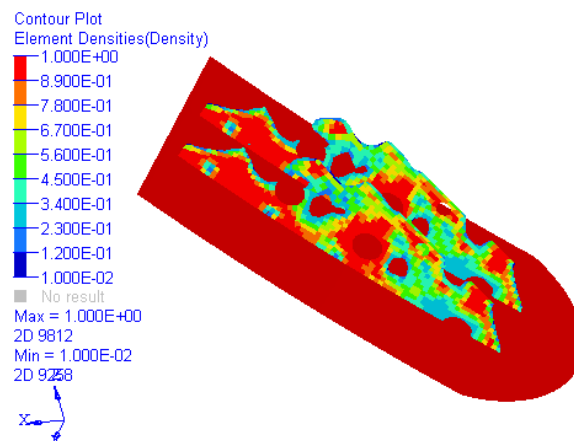


Figure 6. Topology optimization results of the longitudinal member

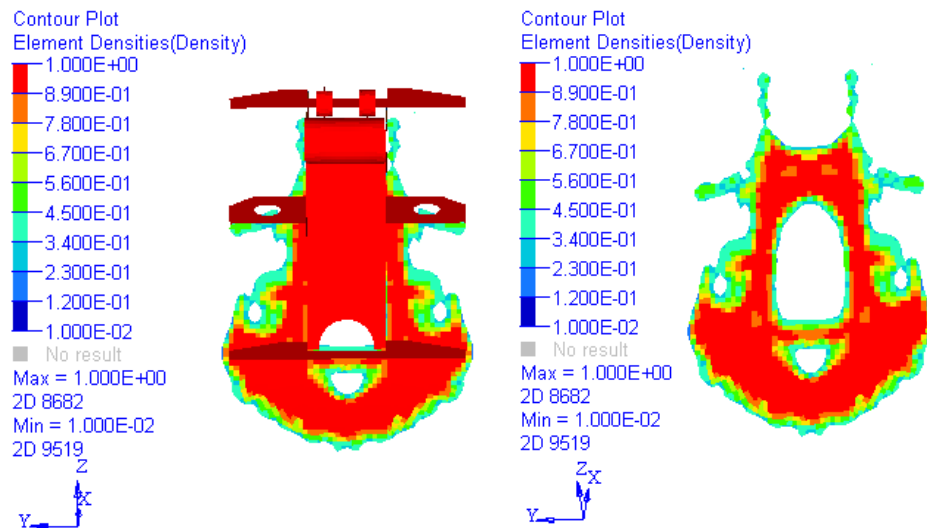


Figure 7. Topology optimization results for the base

4.3. Optimization design of the cover plate

The topology and bead optimization results may be introduced by utilizing the post-processing module OSSmooth of Hypermesh into Catia for design reference in accordance with some certain unit thresholds. The optimization design processes of the cover plate shall satisfy the following conditions:

- (1) The optimized cover plate structure form shall conform to the functional requirements;
- (2) The re-constructed design parts may be processed; and
- (3) The spoiling effects of the operating processes of the optimized cover plate shall be small as can as possible.

By taking the above three requirements, the optimized over plate structure is shown in Figure 8. Because the structure form of the base of the cover plate is matched with the contour of the marine platform, it shall be maintained during the optimization design processes and the stiffeners shall be welded between the base and longitudinal members of the cover plate in accordance with optimization results; and the stiffener structure is shown in Figure 9. Whose thickness is 6mm. the vertical size of longitudinal members may be reduced due to increasing stiffeners; and the thickness of longitudinal members is corrected as 8mm from 6mm to weaken the influence of the cover plate stiffness due to lowering the vertical size of the longitudinal members.

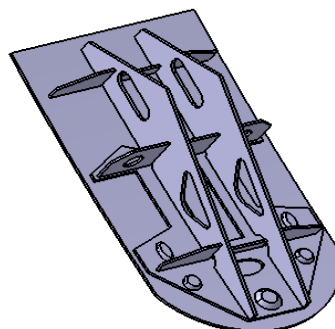


Figure 8. Geometric model of the constructed cover plate

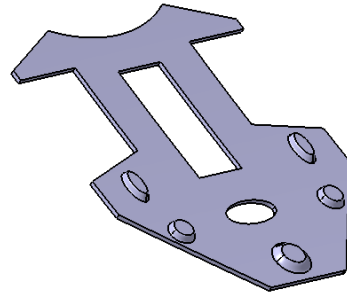


Figure 9. Stiffener structure schematic diagram

4.4. Verification of optimization results

The 3D model of the optimized cover plate is introduced into Hypermesh to establish the FEM model as shown in Figure 10. Various parts of the cover plate were simulated as plate-shell units and stiffeners and the base were connected with Rigid units; and the model includes 10332 units in total. The early 45-order free modal frequencies and strain energies are calculated.

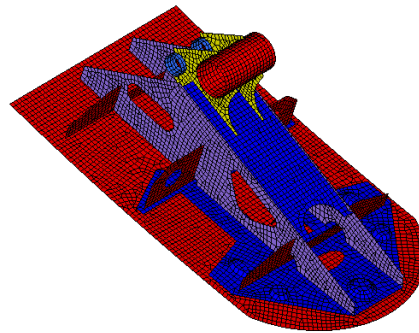


Figure 10. FEM model of the optimized cover plate

Figure 10 presents comparison of inherent frequency of the cover plate before and after optimization. As for the calculated the early 45-order free modes of the cover plate, the early 6-order modes are rigid body modes and the corresponding inherent frequency is 0; thus, the 7th-order mode is equivalent to the 1st-order mode. Figure 10 may indicate that each-order inherent frequency of those of the early 39-order modes of the optimized structure is higher than that of the structure without optimization to effectively prevent the structure resonance even and the system vibration; moreover, the flexibility of the optimized cover plate falls to 31.5N mm from 55N mm but the structure stiffness rises by 57% than that of the structure without optimization; In addition, the increasing stiffness may further weaken the cover plate vibration to improve the vibration performances of the system. Comparison of weights of the cover plate before and after optimization may indicate that the optimized structure stiffness and inherent frequency rise at the same time and the mass growing rate is very small (mass growth: about 5.8kg) as shown in Figure 11.

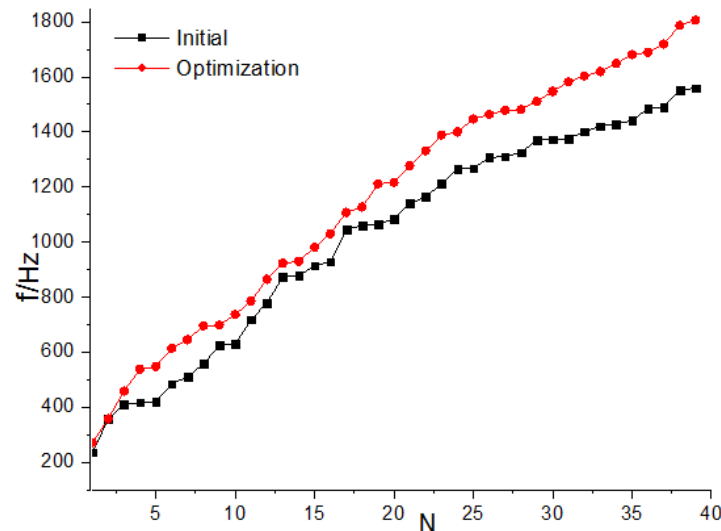


Figure 11. Comparison of the early 45-order inherent frequencies before and after optimization

5. Conclusion

The mode synthesis method was utilized in this study to first theoretically analyse causes for influencing the system vibration performances and obtain maximum structure space for improving the system vibration performances to the greatest extent and optimization of the cover plate. Then the FEM method was adopted to calculate the fluid excitation frequency band. Moreover, the multi-objective bead and topology optimization methods were utilized in this study to improve the cover plate stiffness and the structure optimization was carried out to the cover plate by combining the exciting frequency to obtain the optimal stiffeners and material distributions of the structure; in addition, the reconstruction design was carried out to the cover plate in accordance with optimization results. Comparison results of the optimized and initial structures of the cover plate indicate that:

- (1) The stiffness of the optimized cover plate rises by 57% than that of the initial structure to effectively reduce vibration responses of the system.
- (2) Each-order inherent frequency of the early 45-order modal frequencies of the optimized cover plate is higher than that of the initial structure to effectively avoid the structure resonance.
- (3) No change of the structure form of the base of the cover plate conforms to the function requirements of the system; moreover, the side geometrical shapes of the cover plate also change slightly; namely the spoiling characteristics of operating processes may be influenced very slightly.

References

- [1] Ishitsuka Makoto, IshiiKazuo. Development of an Underwater Manipulator mounted for an AUV. Department of Brain Science and Engineering, Proceedings of MTS/IEEE Oceans, 2005: 164 ~170.
- [2] Y.E. Idar, L.Kjetilf. The hydrostatic corer Selcore-a for sediment sampling and geophysical site characterization. IEEE Trans. AC, 2006, 53(6):123~135.
- [3] J.A. Jahnke. A gravity driven, hydraulically-damped multiple piston corer for sampling fine-grained sediments. Trans. Amen Fish. Soc, 1997, 26(5):66~65.
- [4] Lars A Krog and Niels Olhoff. Topolog Optimization of Integral Rib Reinforcement of Plate and Shell Structures with Weighted-Sum and Max-Min Objectives [J]. Solid Mechanics and its Applications, 1996, 43:171-179.

- [5] Seungjae Min, Shinji Nishiwaki, Noboru Kikuchi. Unified Topology Design of Static and Vibrating Structures Using Multi-objective Optimization [J]. Computers and Structures, 2000, 75:93-116.
- [6] Murali M.R. Krishna. Topology & Topography Optimization of a Drive Shaft[J]. SAE Technical Paper Series 2005-01-3552.
- [7] Yang Dai and Das M. Ramnath A. Topographically Structural Optimization Methodology for Improving Noise Radiation in Transaxles [J].SAE Technical Paper Series 2007-01-2287.
- [8] Mallikarjuna Bennur. Superelement, Component Mode Synthesis, and Automated Multilevel Substructuring for Rapid Vehicle Development [J].SAE Technical Paper Series 2008-01-0287.
- [9] Hurty W C. Vibrations of Structural Systems by Component Mode Synthesis[J]. Journal of the Engineering Mechanics Divion, ASCE, 1960, 86: 51-59.
- [10] Gladwell G M L. Branch Mode Analysis of Vibrating Systems[J]. Sound Vibration. 1964, 1: 41-59.
- [11] Hurty W C. Dynamic Analysis of Structural Systems Using Component Mode [J]. AAIA Journal. 1964, 3 (4): 678-685.
- [12] Craig R R Jr, Bampton M C C. Coupling of Structures for Dynamic Analyses[J]. AAIA Journal. 1968, 6 (7): 1313-1319.
- [13] Deng, M. and Lan, J. The Topology Optimization Analysis On Rope-Wheel Glass Lifter[J]. SAE Technical Paper 2016-01-1384.
- [14] M. P. Bendsøe, O. Sigmund. Material interpolation schemes in topology optimization[J]. Archive of Applied Mechanics, 1999(69):635-654.
- [15] O. Sigmund. A 99 line topology optimization code written in Matlab [J]. Struct Multidisc Optim, 2007(21):120-127.
- [16] Sigmund O. and Petersson J. Numerical instabilities in topology optimization: a survey on procedures dealing with checkerboards, mesh-dependencies and local minima. Structural Optimization, 1998, 16: 68~75
- [17] E. Andreassen, A. Clausen, M. Schevenels, B.S. Lazarov and O.Sigmund. Efficient topology optimization in MATLAB using 88 line of code [J]. Struct Multidisc Optim ,2011,1 (43):1-16.